(2)

STRUCTURAL AND ELECTRICAL PERFORMANCE CONSIDERATIONS IN THE DESIGN OF MULTIBAND RADOMES

G. Dailey and R. C. Mallalieu
The Johns Hopkins University Applied Physics Laboratory
Laurel Maryland

14 May 81

ABSTRACT

Multimode guidance capability is a requirement for missiles that will satisfy the Navy's near- and far-term area defense needs, which implies the use of thin walled radomes on missiles that will operate at speeds up to M8. Structural analyses were conducted to determine the minimum wall thicknesses that are required to carry the aerodynamic loadings during sea level flight at speeds from M2 to M6 undergoing a 30g maneuver. In this paper the results of the parametric loads and stress investigation are discussed. Also covered are the results of an investigation into the electrical performance of three different wall configurations for use with dual-band guidance at 3 and 5 GHz.

INTRODUCTION

Three radome shapes were investigated, von Karman with length-to-diameter ratios (ℓ/d) of 2.1 and 3.0, and a hemispherical ℓ/d of 0.5. Of interest were base diameters of 7.5, 13,5, and 19.5 in. and flight Mach numbers of 2, 4, and 6. The materials of interest were Pyroceram 9606, reaction-sintered silicon nitride (RSSN), hot-pressed silicon nitride (HPSN), slip-cast fused silica (SCFS), and quartz polyimide (QPI). Thus there were three ℓ/d's, three diameters, three Mach numbers, and five materials, total of 135 cases.

Calculations of aerodynamic loads and centers of pressure were made (Reference 1) and used to define minimum wall thicknesses to carry the bending moments resulting from these loads. Also, using the HIMACH code (Reference 2) at NSWC/Dahlgren, pressure distributions were computed on several radomes at various angles of attack. After programming the von Karman radome geometry for the SATANS computer code (Reference 3), some of these cases were explored to determine the wall thicknesses required to prevent buckling. The mechanical analysis indicated that relatively thin ceramic radomes can withstand the assumed flight environments and that structural failure may be due to either buckling or excessive stress at the base of the radome.

The work described in this was performed under the sponsorship of the Surface Warfare Systems Research and Technology Office (62R) of the Naval Sea Systems Command (Contract No. N00024-81-C-5301). Mr. L. Pasiuk (SEA 62R) was the program manager and Dr. F. Moore (NSWC) was the program sponsor.

In the electrical performance investigation a dual-band missile allowing 3 GHz passive guidance combined with 35 GHz terminal homing was assumed. For this concept an 0.078 inch halfwave Pyroceram radome was compared to fullwave and half-sandwich designs. The halfwave radome is sturdy enough to survive a variety of missions, but it is considered too fragile to survive the stresses of fabrication and military handling. However, the electrical evaluation showed that the performance of the halfwave radome far exceeded that of the thicker alternatives. Its bandwidth was about 5% at 35 GHz compared to 2% for the others. Even within their passbands, the boresight errors of the fullwave and half-sandwich will probably be twice those of the halfwave. If high frequency systems are to be utilized, methods must be found to allow the fabrication and handling of thin ceramic radomes.

LOADS AND STRESS ANALYSIS OF RADOME BASE

The aerodynamic loads on a missile are schematically shown in Figure 1, where N is the normal force, D is the drag force, and $\bar{x}$ and $\bar{y}$ give the location of the center of messure. The missile was assumed to be undergoing a sea level 30 g maneuver in order to get the maximum aerodynamic loads on the radome. The angles of attack necessary to pull the 30 g maneuver and the resulting aerodynamic loads were computed using standard missile weights and aerodynamics by Marley (Reference 1). It is assumed that the distance $\bar{y}$ is small and that the contribution to the moment at the base from drag is small. The inertial loads are also assumed to be small and are neglected.

The stress at the base of the radome due to bending moment and axial drag loading is therefore (Reference 4)

$$\sigma = \pm \frac{M_B}{\pi R^2 t} - \frac{D}{2\pi RT} \tag{1}$$

where σ is the stress, M_B the bending moment at the base $(N\bar{x})$, R the base radius, and t the radome thickness. To determine the strength requirement for a radome it has been found convenient to express the above in a more generalized parametric form given below:

$$\frac{\sigma_u}{R} = \frac{FS}{\pi R^2}\left[\pm \frac{M_B}{\pi R} - \frac{D}{2}\right] \tag{2}$$

where σ_u is the ultimate strength of the radome material and FS is the ultimate factor of safety.

The required values of $\frac{\sigma_u t}{R}$ as calculated from equation (1) are given in Table 1 with a factor of safety of 1.25 and are plotted versus Mach number in Figures 2 and 3 for all the different configurations. If the angle of attack is independent of diameter then the curves of Figures 2 and 3 reduce to a single curve for each value of ℓ/d. These results are expressed in general terms and are dependent upon the radome's material properties.

BUCKLING ANALYSIS

For thin-walled radomes under aerodynamic loads, failure due to buckling must be considered. Although a radome made of a brittle material will not buckle in the classic sense, impending buckling will cause stress failures. In order to study buckling of thin-walled radomes, the SATANS computer program (Reference 3) was used. The SATANS program solves geometrically nonlinear, arbitrarily loaded shells of revolution. It uses finite differences in the meridional coordinate and a Fourier expansion in the circumferential coordinate. In the linear case, the total solution is the sum of the solutions for the circumferential modes, but, for the nonlinear case, coupling occurs between the fourier modes. The SATANS program solves the geometrical nonlinear equilibrium problem rather than the eigenvalue problem. For a perfect shell subject to a perfectly symmetrical load, there is no coupling between Fourier modes and buckling will not occur. The method used to obtain buckling loads is to introduce an imperfection in the load of the form

$$\varepsilon C_0 \cos n\theta, \tag{3}$$

where ε is a small number, C_0 is the Fourier coefficient for the zeroth mode, and n is the mode number for which the buckling load is wanted.

The aerodynamic loads were calculated using the HIMACH code (Reference 2) at NSWC. This code calculates the pressure coefficient, C_p, over the entire radome. The pressure coefficient is calculated as a three-term Fourier series,

$$C_p\ (X, \theta) = C_0(X) + C_1\ (X) \cos \theta + C_2(X) \cos 2\theta.$$

The three functions, $C_0(X)$, $C_1(X)$, and $C_2(X)$, are read into the SATANS program and used to define the loading distribution. For most of the SATANS runs, four circumferential modes were used:

0, 1, 2, n,

where the load on mode n is defined by Equation 3.

The equations defining the geometry of the von Karman radome have been derived in the Appendix of Reference 5. These equations defining radius, radii of curvature, etc. have been programmed into the SATANS code.

For the base bending stress case, the important generalized parameter was $\sigma_u t/R$; however, for the buckling case it is Et^3/R^3 (the bending stiffness of the shell divided by R^3). The reason for dividing by R^3 is that for shells of the same shape but different size subject to similar loads, if the value of Et^3/R^3 is the same, the buckling load will be the same. From the results from the SATANS code, this generalized buckling parameter (Et^3/R^3) and a parameter referred to as the load factor are plotted in Figure 4 for the lowest buckling modes. The load factor is defined as the ratio of the applied load to the nominal load. Therefore, since a factor of safety of 1.25 is assumed to be the design requirement, the value of Et^3/R^3 at a load factor of 1.25 is used to calculate the required wall thickness for each material.

In Figure 4 note that all but one of the SATANS runs were made with a diameter of 19.5 in. This was done as an economy move to keep the number of runs to a minimum. It has been assumed that the effect of angles of attack is small and that the critical load versus Et^3/R^3 is independent of size. One run was made to check this assumption. The results for the 7.5 in. diameter radome do fall

on the curve for the 19.5 in. diameter radome. The required values of Et^3/R^3 for a load factor of 1.25 have been included in Table I. In this table only the $\ell/d = 3.0$ von Karman radome has a full set of values and no values are present for the hemispherical radome.

In Figure 5 the modal deflection curves for a typical SATANS run at Mach 6 are shown. Note that the curve for mode 4 becomes flat before the SATANS run stops. Near the buckling load the deflection for mode 4 changes a lot for a very small change in load.

CALCULATION OF MINIMUM WALL THICKNESS

The generalized results of the analyses are summarized in Table 1. Here the generalized parameters are $\sigma_u t/R$ for base bending stress and Et^3/R^3 for buckling. The radomes are assumed to have reached equilibrium temperatures at the time the loads are applied. For the five materials considered in this study, the ultimate stress in both tension and compression and the modulus of elasticity at the approximate equilibrium temperature are considered. Using the material property data of Table 2 and the generalized parameters from Table 1, the minimum wall thickness were calculated. The resultant wall thicknesses are shown in Table 3, and for Pyroceram 9606 they are shown in Figure 6.

ELECTRICAL CONSIDERATIONS FOR A HIGH-FREQUENCY CERAMIC RADOME

One attractive combination of guidance modes is passive guidance at frequencies on the order of 3 GHz followed by active guidance (transmitter and receiver on the missile) at a much higher frequency, perhaps 35 GHz. The most stringent requirements for the dual-band radome are at the high terminal frequency. There are:

1) Low insertion loss to allow timely detection.

2) Low radome refraction (boresight errors) to prevent steering instabilities.

3) Transmission relatively independent of changes in incident polarization.

The first requirement means that the radome wall structure must be designed to minimize microwave reflections since these are far more significant than material resistive heating. For a single layer radome, this restricts operation to passbands about the thin wall, halfwave, or multiple halfwave modes. Within these passbands, the other design objectives are primarily determined by the type of radome wall and the dielectric constant (ε) of the material.

The solid wall halfwave radome is by far the most attractive for single-band operation. Although its bandwidth is only 5%, its high transparency, low refraction, and favorable polarization properties make it a useful standard of comparison for other radome designs. The thinwall radome operates as a low-pass filter. Thus, a single layer radome could operate as a halfwave radome over a 5% band at 35 GHz and as a thin wall at frequencies up to one-tenth that or 3.5 GHz. This would appear to be an optimum choice for the dual-band radome.

Unfortunately, a ceramic radome is exceedingly thin at 35 GHz. For a radome operating in the N-halfwave mode and at a design angle of incidence θ, the thickness is:

$$t = \frac{Nc}{2f\sqrt{\varepsilon - \sin^2\theta}}$$

The design angle must be chosen to allow transmission over the near grazing angles encountered within a streamlined radome. For Pyroceram 9606 (ε= 5.53) and $\theta = 73^\circ$, panel thickness is only 0.078 inches. While the first portion of this study has indicated that such a radome could survive the flight stresses of many of the cases described, it is considered by some to be too thin to allow commercial fabrication and military handling. Its electrical performance should be evaluated and compared to the alternatives. If the performance penalty for the alternate designs is excessive, perhaps techniques may be devised to overcome the problems of manufacturing and handling such a radome.

The halfwave Pyroceram radome is evaluated in comparison to a fullwave of the same material and also to a half-sandwich design. The latter consists of an outer layer of Pyroceram backed up by a sufficient thickness of ceramic foam to maximize transmission. The thickness of the outer layer was set to 0.100 inches, the minimum considered allowable for fabrication and handling considerations. All radomes were designed for maximum transmission at 35 GHz and 73°.

The relative quality of these radome walls may be evaluated by the calculated loss and insertion phase delay (IPD) of large flat panels. Loss should remain low for angles of incidence between 40 and 80 degrees. Radome refraction, or boresight error, is primarily caused by the slope of the (IPD) characteristic with angle of incidence. This deflects the beam in a similar fashion to the bending of light by a prism. The third design objective, insensitivity to polarization, depends upon the spread between the transmission characteristics for parallel and perpendicular polarization.

Figure 7 shows the transmission of a 0.078 inch halfwave panel of Pyroceram 9606 at the design frequency and at $\pm$5% offsets. The center figure, at the design frequency, serves as the standard of comparison. As required, loss remains low over the critical high angles of incidence. The slope of the IPD curves is acceptable according to the low levels of boresight error associated with halfwave radomes. Both loss and IPD curves track as a function of polarization.

Figure 7's two outer diagrams show the detuning of the panel with frequency. These 5% frequency offsets are excessive for a halfwave radome, in which total bandwidth is about 5%. These offsets were chosen to emphasize changes in transmission with frequency. Loss increases for the perpendicular component, and the curves no longer track with polarization.

Figure 8 shows the transmission of a 0.157 inch fullwave panel of Pyroceram 9606. It also was designed for 35 GHz and 73°. At 35 GHz, insertion loss is significantly higher than the halfwave except in the vicinity of the design angle. The slopes of the IPD curves are twice those of the halfwave. Even at the design frequency, the resulting boresight errors would be about twice those of the halfwave. The outer diagrams of Figure 8 show a severe detuning for 5% frequency offsets.

Figure 9 represents the half-sandwich with a 0.100 outer layer of Pyroceram and an inner layer of ceramic foam ($\varepsilon = 3.0$, $\tan\delta = 0.01$) in which the 0.076 inch foam thickness was adjusted to maximize transmission at 35 GHz and 73°. A comparison of Figure 9 and Figure 8 shows that the transmission of this half-sandwich approximates that of the fullwave. The only noticeable exception is the higher loss of the parallel polarization component. This is due to the relatively high loss tangent assumed for the foam layer.

The two-layer half-sandwich has sometimes been called a "broadband" radome. In comparison to typical broadband panels, the thinwall, the A-sandwich and the C-sandwich, which offer broadband transmission for relatively low angles of incidence, Figure 9 shows that the half-sandwich approximates the relatively narrow-band performance of the fullwave. What then are its advantages? As a general rule, the presence of the foam layer behind a relatively thin outer layer of higher ε material makes the panel operate like the next higher N-halfwave wall. This may be advantageous in the following situations:

1) If the hard outer layer is made of a material which is expensive, a minimally thick outer wall may be combined with a less expensive inner layer.

2) The passband is somewhat great than that of the N-halfwave because of the decrease in average dielectric constant, but the mid-band performance will be slightly inferior to that of the N-halfwave panel. However, the half-sandwich is not a broadband radome.

The bandwidth of the halfwave, fullwave and half-sandwich panels are compared in Table 4. The phasor sum of the complex transmission coefficients for ten representative rays was calculated. These are parallel and perpendicular polarized rays at angles of incidence of 60, 65, 70, 75 and 80 degrees. At 3 GHz, all three panels would be satisfactory since insertion loss is not critical for passive guidance. According to loss considerations, the 35 GHz bandwidth of the halfwave radome is much wider than that of either of the alternatives. Since IPD slope variations would reduce bandwidth still further, the total bandwidth of the fullwave and the pseudo fullwave half-sandwich will only be about 2%, compared to the typical halfwave radome bandwidth of 5%.

DISCUSSION AND CONCLUSIONS

It is apparent from the results in Table 2 that, in general, both buckling and base bending stress should be considered in designing thin-walled radomes. The results do not vary much from configuration to configuration, and the conclusions reached regarding the importance of base stress versus buckling are independent of the configuration.

Several of the materials considered cannot withstand the equilibrium temperatures associated with the higher sea-level Mach numbers. The QPI cannot operate at equilibrium temperatures associated with Mach 4 and 6 and is buckling limited at Mach 2. The SCFS cannot operate at the Mach 6 equilibrium temperature and is stress-limited at Mach 2 and 4. Pyroceram 9606, RSSN, and HPSN all have the same characteristics - buckling controls the design at Mach 2, stress controls the design at Mach 6, and either may control at Mach 4. Thus, for these three materials, both failure modes must be considered.

If radome fragility during fabrication and handling is used to establish the minimum practical thickness for ceramic radomes, the performance penalty during active homing at 35 GHz could be quite high. The electrical performance of the fullwave and half-sandwich radomes are far inferior to that of the 0.078 inch halfwave. For a fixed diameter seeker, boresight errors and slopes appear to decrease somewhat with large increases in frequency for systems which use halfwave radomes. Thus, for a relatively large missile, the higher IPD slopes of the fullwave and half-sandwich radomes may be tolerable. The restricted bandwidth still remains, however, and this may make the system more vulnerable to secondary effects such as radome de-tuning due to aerodynamic heating.

References

1. E. T. Marley, "Calculation of Aerodynamic Loads and Centers of Pressure on a Series of Designated Radomes", JHU/APL BFD-EM-986, March 1980.

2. J. Sun, "User's Guide and Assessment of the NCSU Body Alone High Mach Code", NSEC K21 No. 2/79, November 1978.

3. R. E. Ball, "A Geometrically Nonlinear Analysis of Arbitrarily Loaded Shells of Revolution", NASA CR-909, January 1968.

4. G. Dailey, "Structural Analysis of Thin Walled Radomes", JHU/APL EM-4943, May 1980.

5. G. Dailey, "Structural Analysis of Three Postulated Radomes for the SS-N-3a Cruise Missile", APL/JHU EM-4567. June, 1974.

Table 1

Summary of Material Strength and Stiffness Requirements for 30 g Sea-Level Maneuver

Case	ℓ/d	d	M	Strength Requirement $\sigma_u t/R$		Stiffness Requirement Et^3/R^3
				Tension	Compression	
Spherical						
1	0.5	7.5	2		25.45	
2	0.5	7.5	4		99.84	
3	0.5	7.5	6		225.75	
4	0.5	13.5	2		25.51	
5	0.5	13.5	4		102.84	
6	0.5	13.5	6		228.18	
7	0.5	19.5	2		25.80	
8	0.5	19.5	4		102.07	
9	0.5	19.5	6		224.76	
Von Karman						
10	2.1	7.5	2	63.50	70.92	
11	2.1	7.5	4	75.80	97.67	
12	2.1	7.5	6	98.19	156.53	3.40
13	2.1	13.5	2	74.46	81.66	
14	2.1	13.5	4	96.72	117.99	
15	2.1	13.5	6	109.05	156.58	3.40
16	2.1	19.5	2	72.29	79.53	
17	2.1	19.5	4	87.97	109.20	
18	2.1	19.5	6	98.20	156.40	3.40
19	3.0	7.5	2	109.44	113.46	7.00
20	3.0	7.5	4	132.17	148.44	2.10
21	3.0	7.5	6	142.30	173.34	3.00
22	3.0	13.5	2	126.13	129.94	7.00
23	3.0	13.5	4	162.82	179.48	2.10
24	3.0	13.5	6	160.72	191.72	3.00
25	3.0	19.5	2	119.50	123.35	7.00
26	3.0	19.5	4	153.81	170.44	2.10
27	3.0	19.5	6	160.52	191.47	3.00

Table 2

Material Properties of Radome Materials
at Equilibrium Temperatures

Ultimate Stress in Tension (psi)

M	T (^{o}F)	9606	RSSN	HPSN	SCFS	QPI
2	400	22 K	20 K	50 K	5 K	45 K
4	1400	12 K	20 K	50 K	5 K	-
6	3000	4.8 K	9.8 K	9 K	-	-

Ultimate Stress in Compression (psi)

M	T (^{o}F)	9606	RSSN	HPSN	SCFS	QPI
2	400	115 K	200 K	200 K	50 K	20 K
4	1400	115 K	200 K	200 K	80 K	-
6	3000	20 K	200 K	200 K	-	-

Modulus of Elasticity (psi)

M	T (^{o}F)	9606	RSSN	HPSN	SCFS	QPI
2	400	15.7×10^6	15×10^6	40×10^6	5×10^6	2×10^6
4	1400	16.7×10^6	15×10^6	35×10^6	5×10^6	-
6	3000	$.9 \times 10^6$	8×10^6	8.6×10^6	-	-

Table 3

Required Wall Thickness for Radomes Subject to Aerodynamic Loads

	9606		RSSN		HPSN		SCFS		QPI	
Case*	TS	TB	TS	TB	TS	TB	TS	TB	TS	TB
1	0.0008		0.0005		0.0005		0.0019		0.0048	
2	0.0033		0.0019		0.0019		0.0047			
3	0.0423		0.0042		0.0042					
4	0.0015		0.0009		0.0009		0.0034		0.0086	
5	0.0060		0.0035		0.0035		0.0087			
6	0.0770		0.0077		0.0077					
7	0.0022		0.0013		0.0013		0.0050		0.0126	
8	0.0087		0.0050		0.0050		0.0124			
9	0.1096		0.0110		0.0110					
10	0.0108		0.0119		0.0048		0.0476		0.0133	
11	0.0237		0.0142		0.0057		0.0568			
12	0.0767	0.0584	0.0376	0.0282	0.0409	0.0275				
13	0.0228		0.0251		0.0101		0.1005		0.0276	
14	0.0544		0.0326		0.0131		0.1306			
15	0.1534	0.1051	0.0751	0.0507	0.0818	0.0495				
16	0.0320		0.0352		0.0141		0.1410		0.0388	
17	0.0715		0.1429		0.0172		0.1715			
18	0.1995	0.1519	0.0977	0.0733	0.1064	0.0716				
19	0.0187	0.0281	0.0205	0.0291	0.0082	0.0210	0.0821	0.0420	0.0213	0.0569
20	0.0413	0.0188	0.0248	0.0195	0.0099	0.0147	0.0991	0.0281		
21	0.1112	0.0560	0.0545	0.0270	0.0593	0.0264				
22	0.0387	0.0505	0.0426	0.0524	0.0170	0.0378	0.1703	0.0755	0.0439	0.1025
23	0.0916	0.0338	0.0550	0.0350	0.0220	0.0264	0.2198	0.0505		
24	0.2260	0.1008	0.1107	0.0487	0.1205	0.0475				
25	0.0530	0.0730	0.0583	0.0756	0.0233	0.0545	0.2330	0.1091	0.0501	0.1480
26	0.1250	0.0488	0.0750	0.0506	0.0300	0.0382	0.2999	0.0730		
27	0.3261	0.1456	0.1597	0.0703	0.1739	0.0686				

*Specifications from Table 1

TS = Thickness required to satisfy the base bending stress (compressive stress limited for all spherical radomes and von Karman radome of QPI; all other von Karman radomes are tensile stress limited).

TB = Thickness required to satisfy buckling.

Table 4

Approximate Radome Insertion Loss (One-Way)

Type	3 GHz	33.25 GHz	35.00 GHz	36.75 GHz
Halfwave	1.6 dB	0.7 dB	0.1 dB	1.0 dB
Fullwave	2.9	1.8	0.3	2.5
Half-Sandwich	2.6	1.7	0.9	2.4

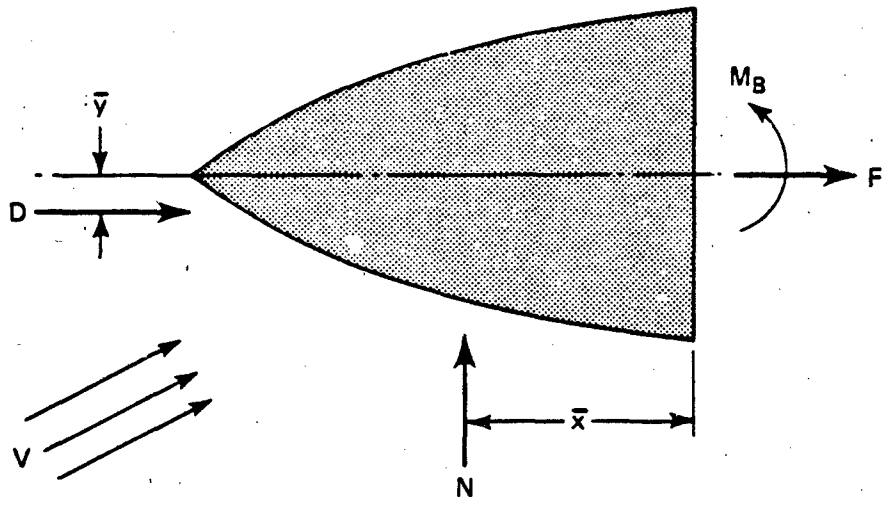

Figure 1 Aerodynamic loads on a radome.

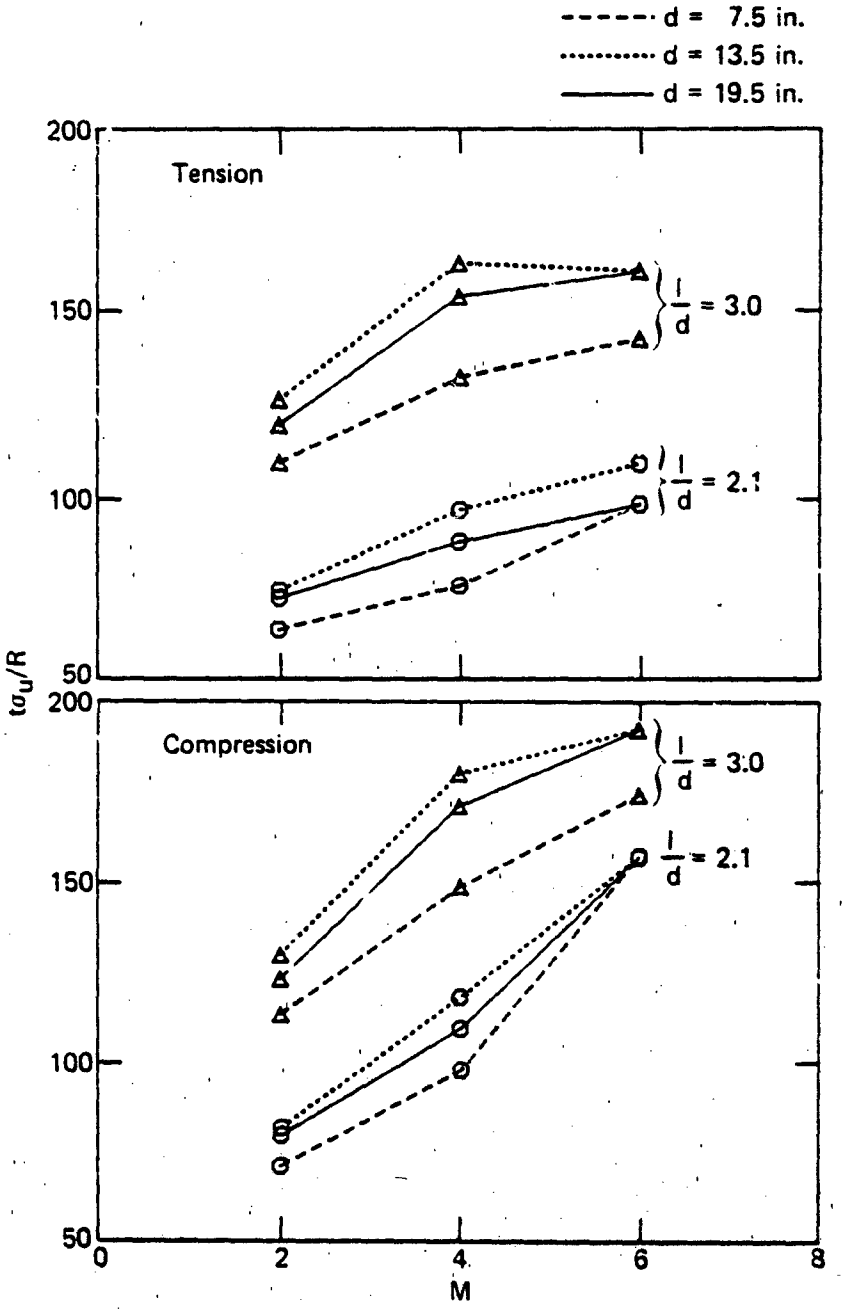

Figure 2 Required wall thickness for stress at base of Von Karman radome.

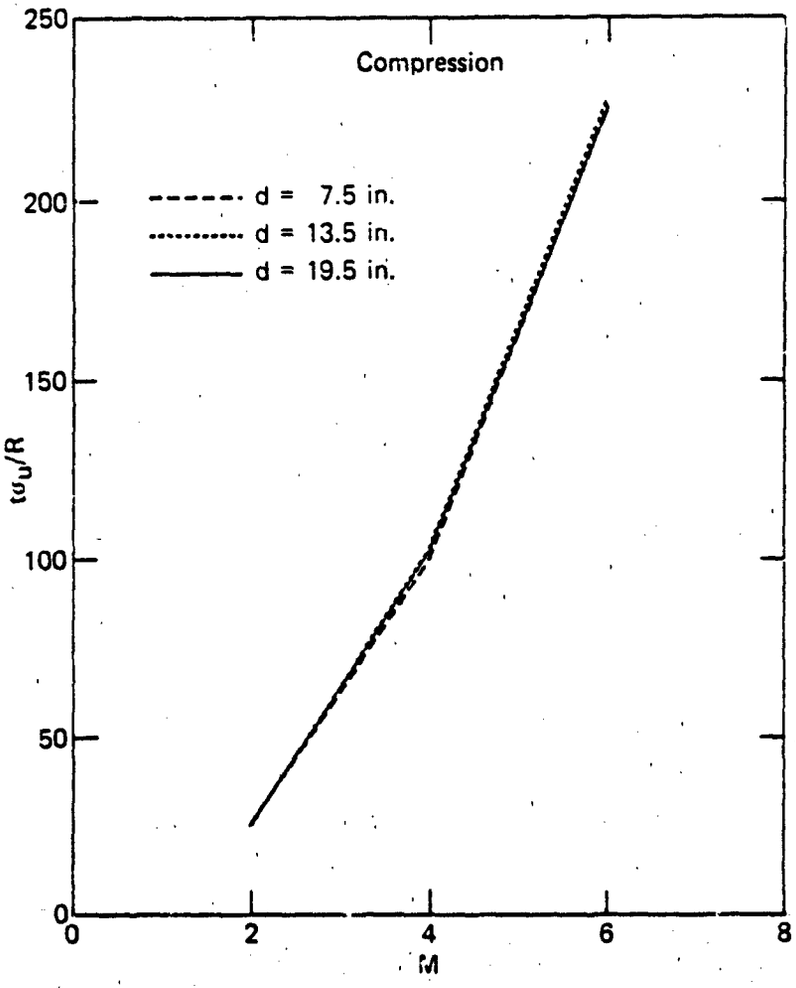

Figure 3 Required wall thickness for stress at base of hemispherical radome.

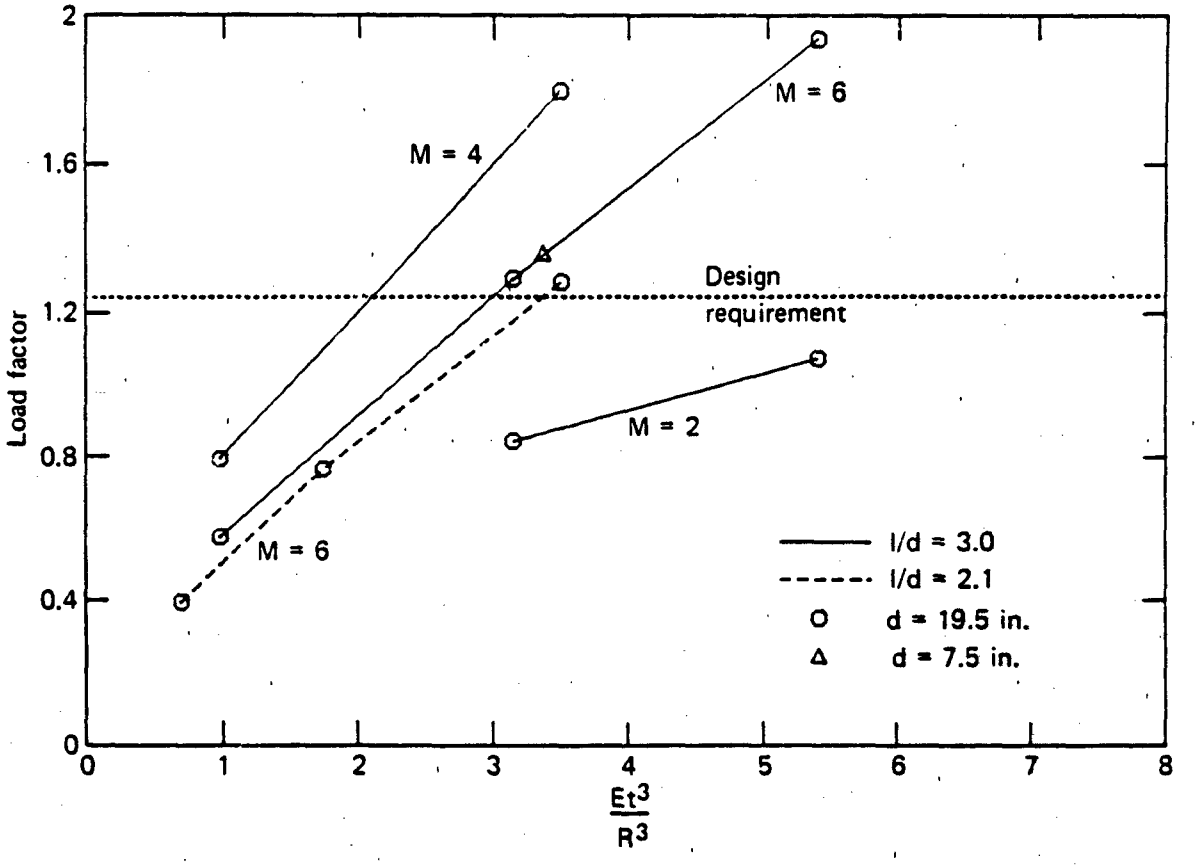

Figure 4 Load factor needed to buckle versus Et^3/R^3 for Von Karman radomes.

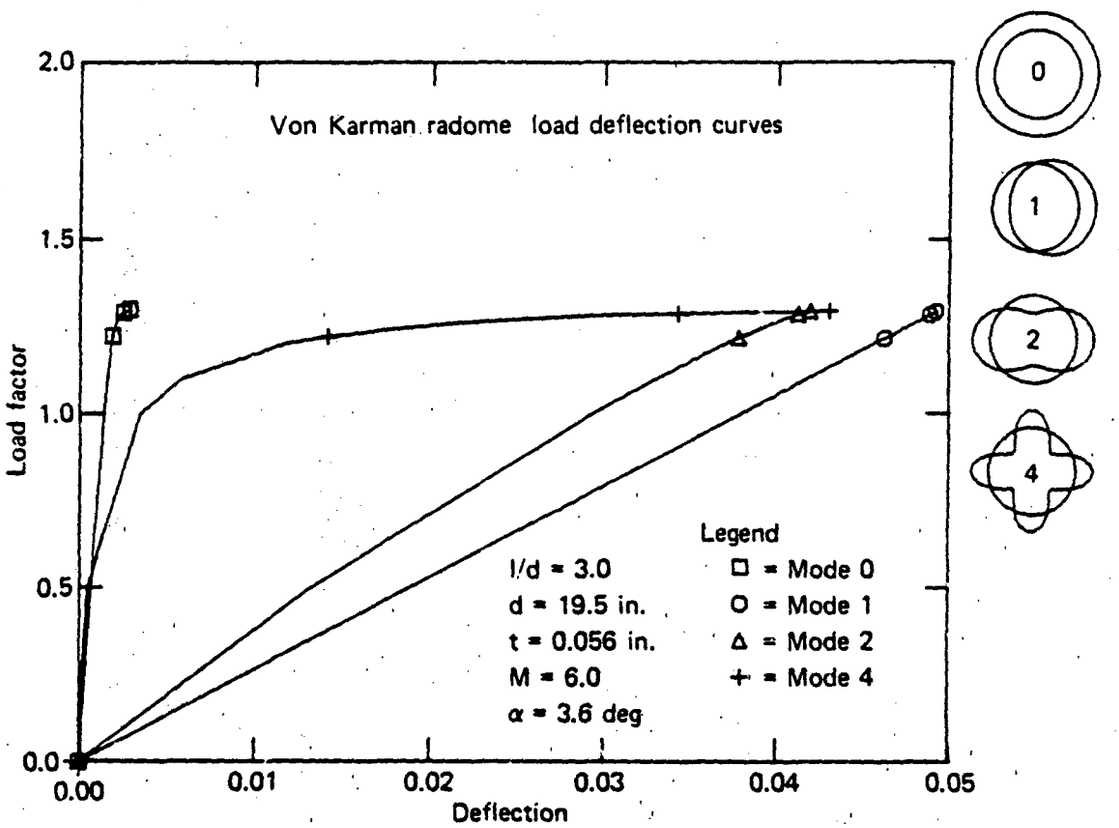

Figure 5 **Load versus deflection for different circumferential modes of a Von Karman radome at Mach 6.**

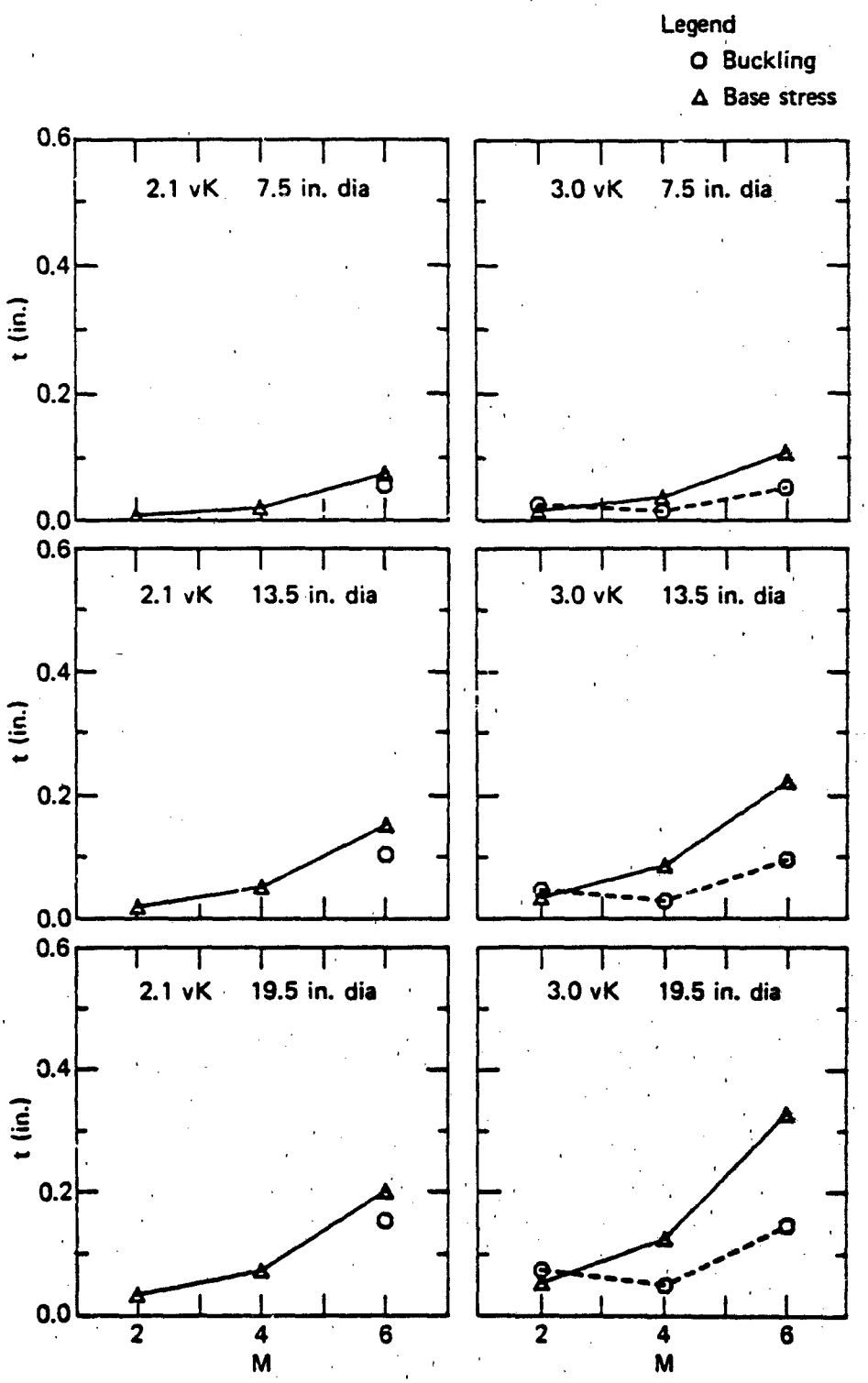

Figure 6 Required wall thicknesses f . Pyroceram 9606 radome subject to aerodynamic loads.

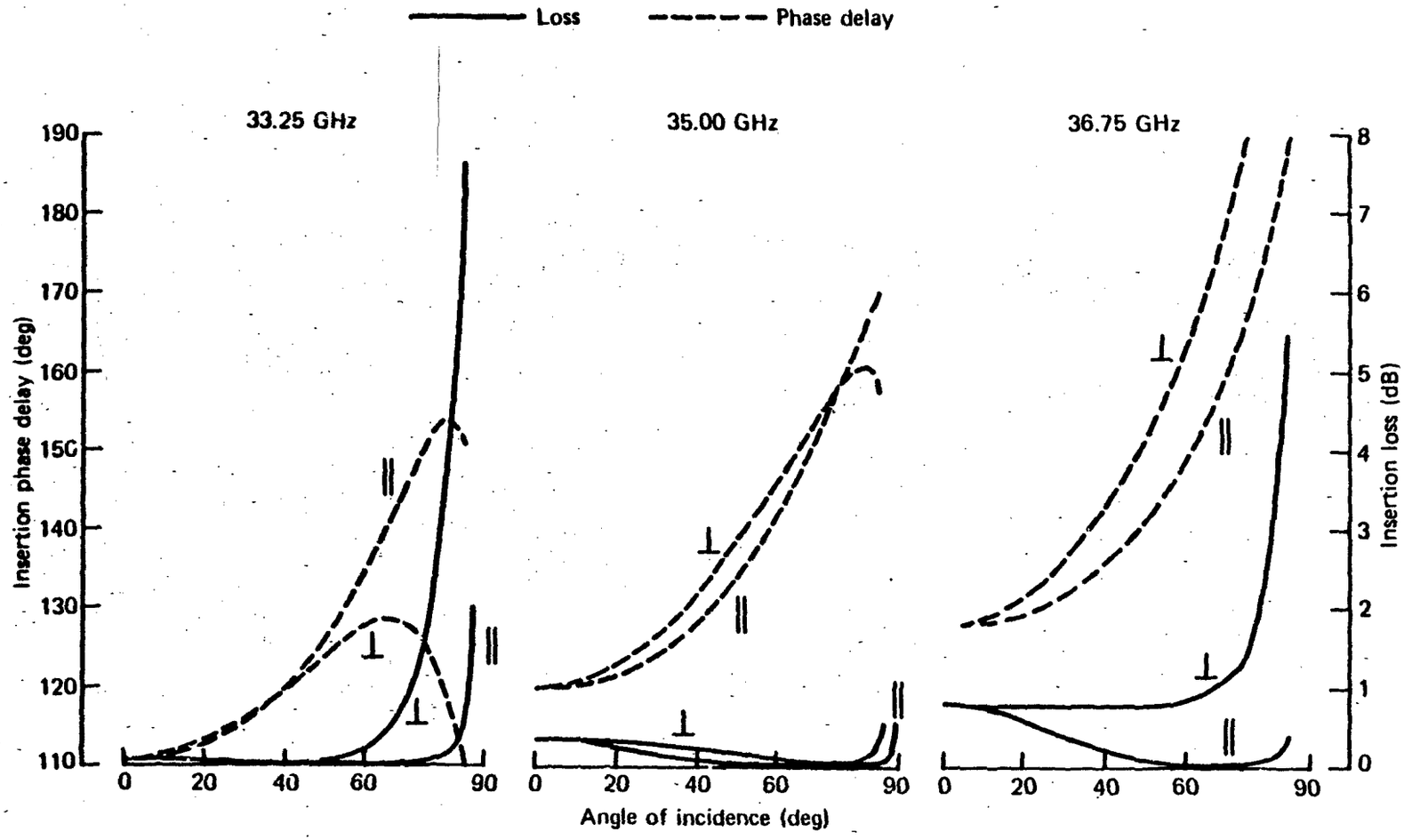

Figure 7 Transmission of halfwave panel.

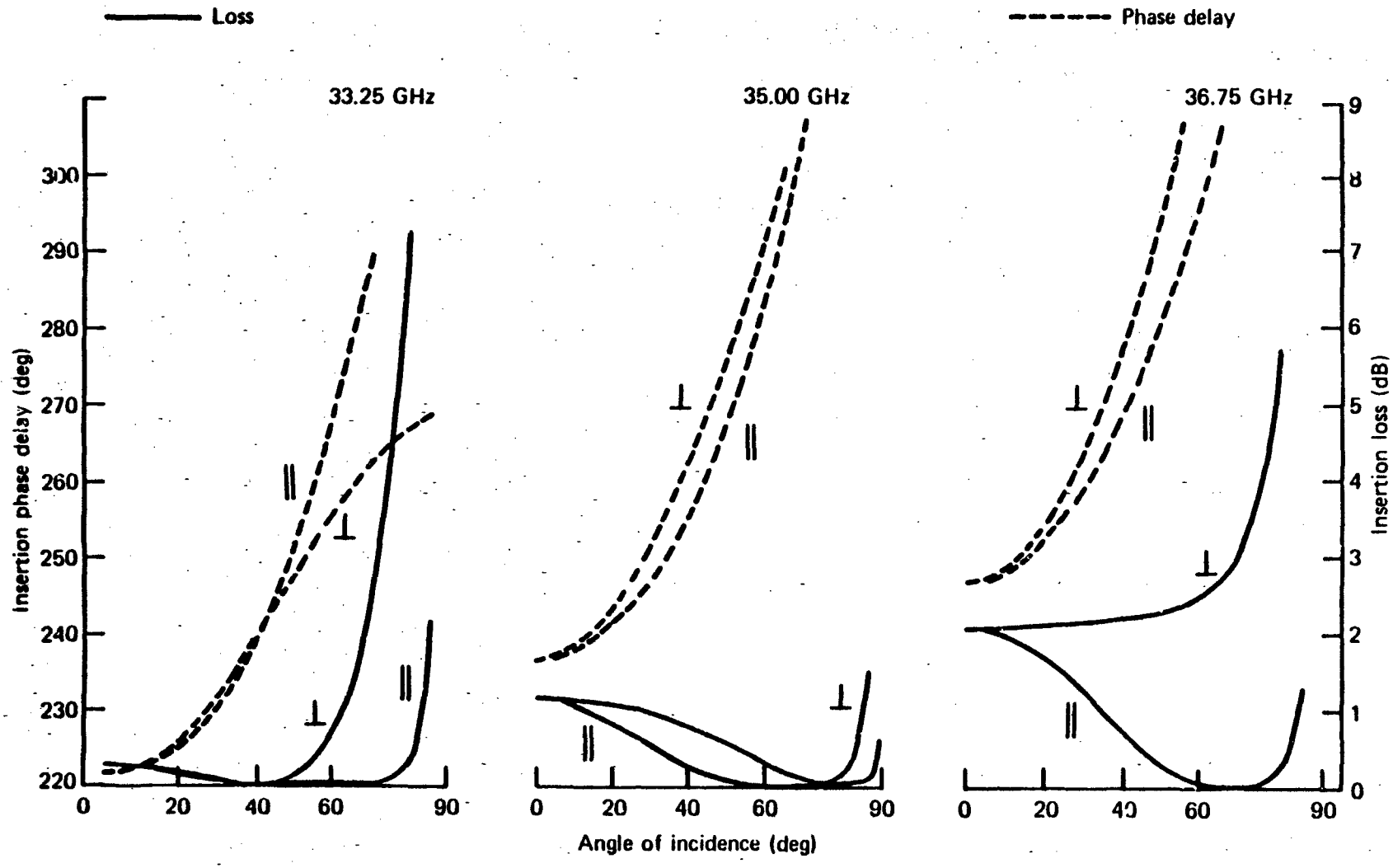

Figure 8 Transmission of fullwave panel.

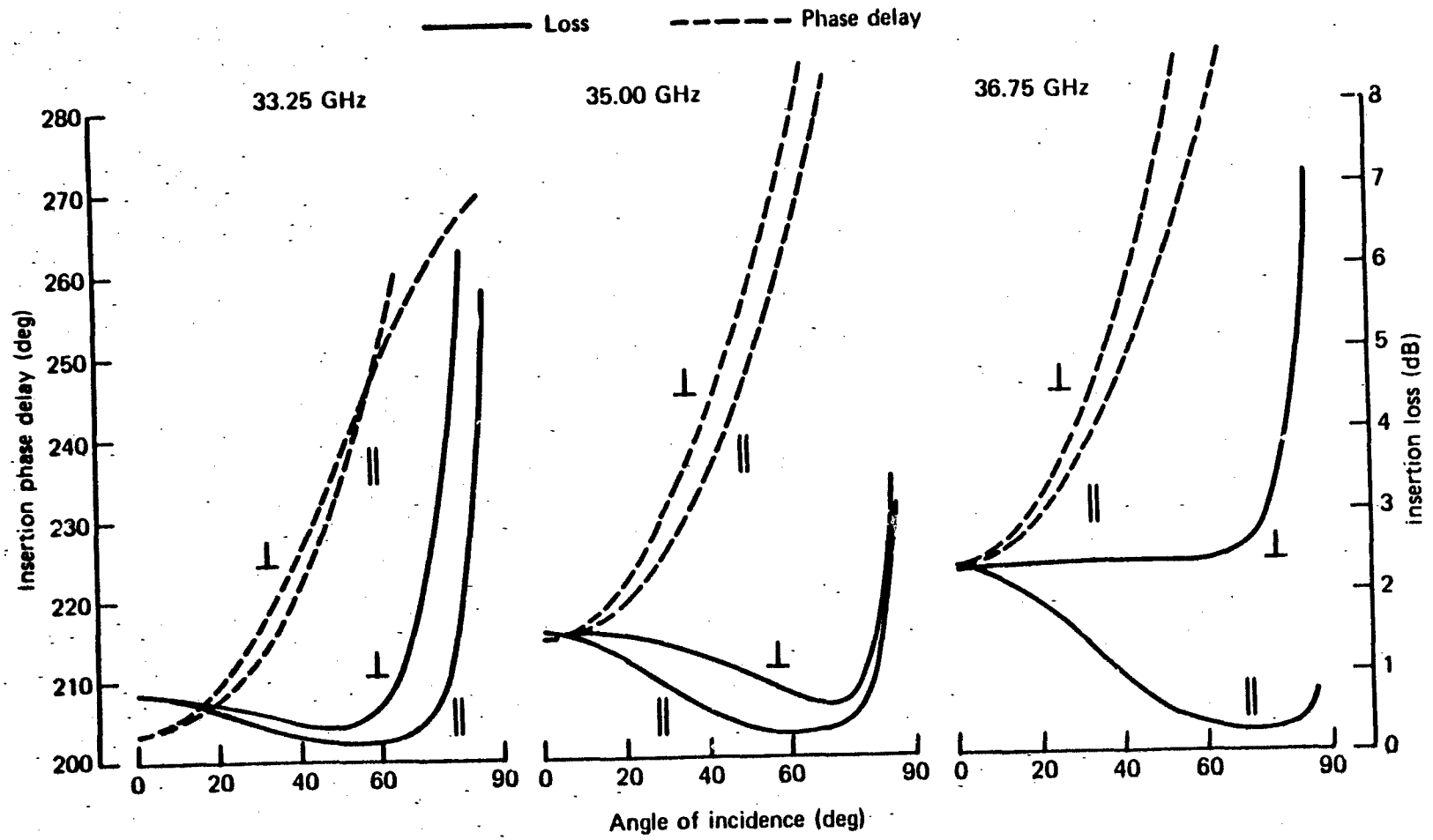

Figure 9 Transmission of halfsandwich panel.